13

Particle Transport Monte Carlo Method for Heat Conduction Problems

Nam Zin Cho
Korea Advanced Institute of Science and Technology (KAIST), Daejeon, South Korea

1. Introduction

Heat conduction [1] is usually modeled as a diffusion process embodied in heat conduction equation. The traditional numerical methods [2, 3] for heat conduction problems such as the finite difference or finite element are well developed. However, these methods are based on discretized mesh systems, thus they are inherently limited in the geometry treatment. This chapter describes the Monte Carlo method that is based on particle transport simulation to solve heat conduction problems. The Monte Carlo method is "meshless" and thus can treat problems with very complicated geometries.

The method is applied to a pebble fuel to be used in very high temperature gas-cooled reactors (VHTGRs) [4], which is a next-generation nuclear reactor being developed. Typically, a single pebble contains ~10,000 particle fuels randomly dispersed in graphite–matrix. Each particle fuel is in turn comprised of a fuel kernel and four layers of coatings. Furthermore, a typical reactor would house several tens of thousands of pebbles in the core depending on the power rating of the reactor. See Fig. 1. Such a level of geometric complexity and material heterogeneity defies the conventional mesh–based computational methods for heat conduction analysis.

Among transport methods, the Monte Carlo method, that is based on stochastic particle simulation, is widely used in neutron and radiation particle transport problems such as nuclear reactor design. The Monte Carlo method described in this chapter is based on the observation that heat conduction is a diffusion process whose governing equation is analogous to the neutron diffusion equation [5] under no absorption, no fission and one speed condition, which is a special form of the particle transport equation. While neutron diffusion approximates the neutron transport phenomena, conversely it is applicable to solve diffusion problems by transport methods under certain conditions. Based on this idea, a new Monte Carlo method has been recently developed [6-8] to solve heat conduction problems. The method employs the MCNP code [9] as a major computational engine. MCNP is a widely used Monte Carlo particle transport code with versatile geometrical capabilities.

Monte Carlo techniques for heat conduction have been reported [10-13] in the past. But most of the earlier Monte Carlo methods for heat conduction are based on discretized mesh systems, thus they are limited in the capabilities of geometry treatment. Fraley et al[13] uses a "meshless" system like the method in this chapter but does not give proper treatment to the boundary conditions, nor considers the "diffusion-transport theory correspondence" to be described in Section 2.2 in this chapter. Thus, the method in this chapter is a transport theory treatment of the heat conduction equation with a methodical boundary correction. The

transport theory treatment can easily incorporate anisotropic conduction, if necessary, in a future study.

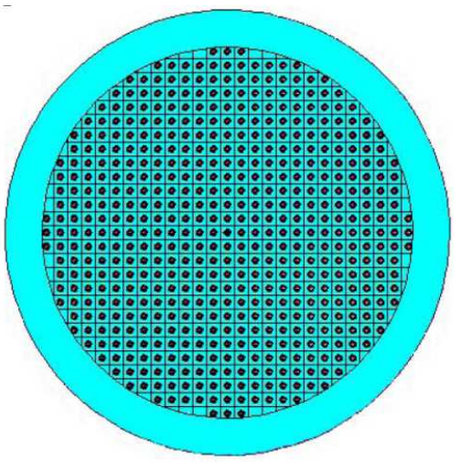

(a) A pebble fuel element

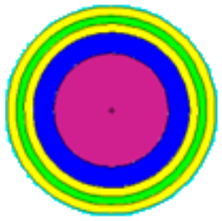

(b) A coated fuel particle

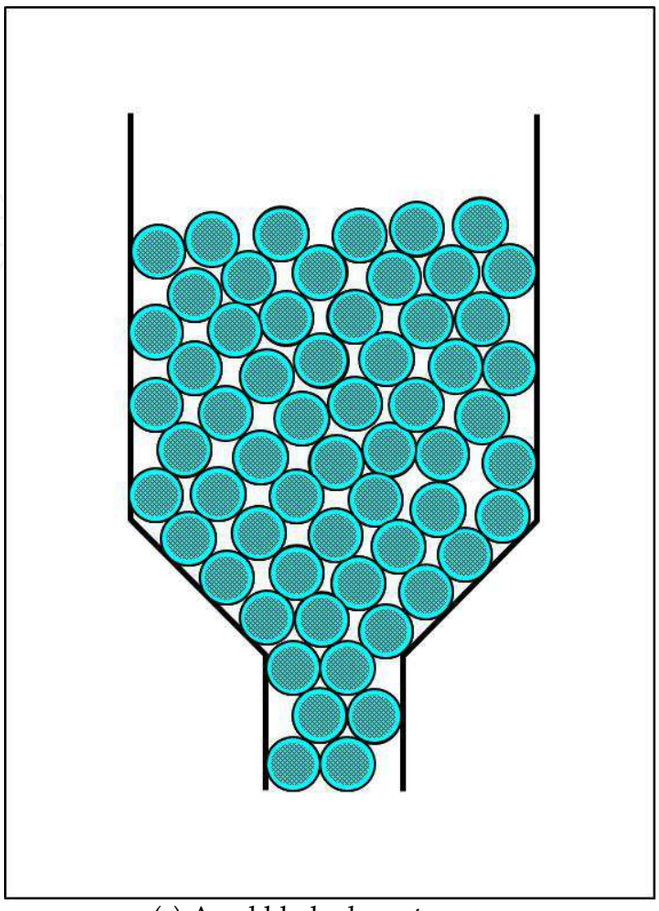

(c) A pebble-bed reactor core

Fig. 1. Cross-sectional view of a pebble fuel (a) consisting several thousands of coated fuel particles (b) in a reactor core (c)

2. Description of method

2.1 Neutron transport and diffusion equations

The transport equation that governs the neutron behavior in a medium with total cross section $\Sigma_t(\vec{r},E)$ and differential scattering cross section $\Sigma_s(\vec{r},E'\to E,\vec{\Omega}'\cdot\vec{\Omega})$ is given as [5]:

$$\vec{\Omega}\cdot\nabla\psi(\vec{r},E,\vec{\Omega})+\Sigma_t(\vec{r},E)\psi(\vec{r},E,\vec{\Omega})=\int dE'\int d\vec{\Omega}'\Sigma_s(\vec{r},E'\to E,\vec{\Omega}'\cdot\vec{\Omega})\psi(\vec{r},E',\vec{\Omega}') + S(\vec{r},E,\vec{\Omega}) \tag{1a}$$

with boundary condition, for $\vec{n}\cdot\vec{\Omega}<0$,

$$\psi(\vec{r}_s,E,\vec{\Omega})=\begin{cases}\psi_s(E,\vec{\Omega}), & given,\\ 0, & if\ vacuum,\end{cases} \tag{1b}$$

where

$$\vec{r} = neutron\ position,$$
$$E = neutron\ energy,$$
$$\vec{\Omega} = neutron\ direction,$$
$$S = neutron\ source,$$
$$\psi(\vec{r}, E, \vec{\Omega}) = neutron\ angular\ flux.$$

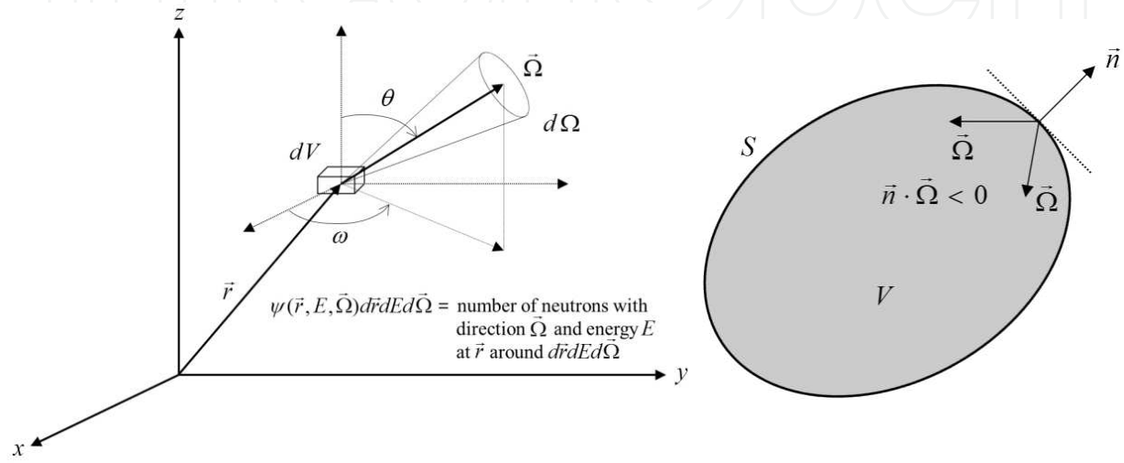

Fig. 2. Angular flux and boundary condition

Fig. 2 depicts the meaning of angular flux $\psi(\vec{r}, E, \vec{\Omega})$ and boundary condition. In the special case of no absorption, isotropic scattering, and mono-energy of neutrons, Eq. (1) becomes

$$\vec{\Omega} \cdot \nabla \psi(\vec{r}, \vec{\Omega}) + \Sigma_s(\vec{r})\psi(\vec{r}, \vec{\Omega}) = \frac{1}{4\pi}\Sigma_s(\vec{r})\phi(\vec{r}) + \frac{S(\vec{r})}{4\pi}, \tag{2a}$$

with vacuum boundary condition,

$$\psi(\vec{r}_s, \vec{\Omega}) = 0 \ for\ \vec{n} \cdot \vec{\Omega} < 0, \tag{2b}$$

where scalar flux is defined as

$$\phi(\vec{r}) = \int d\vec{\Omega}\psi(\vec{r}, \vec{\Omega}). \tag{2c}$$

Let us now consider a "scaled" equation of (2a),

$$\vec{\Omega} \cdot \nabla \psi(\vec{r}, \vec{\Omega}) + \beta\Sigma_s(\vec{r})\psi(\vec{r}, \vec{\Omega}) = \frac{1}{4\pi}\beta\Sigma_s(\vec{r})\phi(\vec{r}) + \frac{1}{\beta}\frac{S(\vec{r})}{4\pi}. \tag{3}$$

An important result of the asymptotic theory provides correspondence between the transport equation and the diffusion equation, i.e., the asymptotic $(\beta \to \infty)$ solution of Eq. (3) satisfies the following diffusion equation:

$$-\frac{1}{3\Sigma_s(\vec{r})}\nabla\phi(\vec{r}) = S(\vec{r}), \tag{4a}$$

with vacuum boundary condition

$$\phi(\vec{r}_s + d) = 0, \quad d = extrapolation\ distance. \tag{4b}$$

It is known that, between the two solutions from transport theory and from diffusion theory, a discrepancy appears near the boundary. Thus, the problem domain is extended using an extrapolated thickness (typically $d \simeq one\ mean\ free\ path = 1/\Sigma_t$) for boundary layer correction, as shown in Fig. 3.

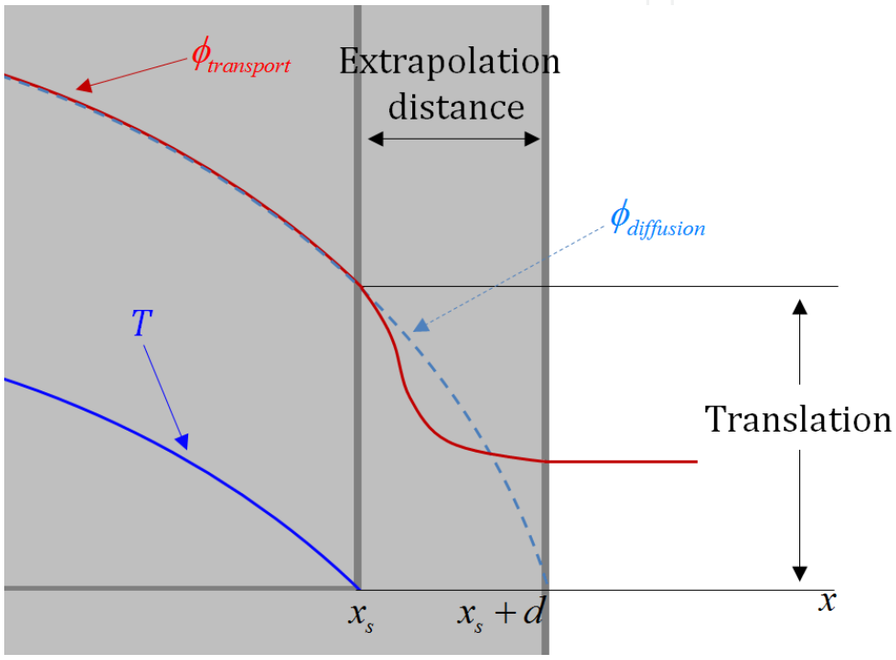

Fig. 3. Boundary correction with an extrapolated layer

2.2 Monte Carlo method for heat conduction equation

Correspondence

The steady state heat conduction equation for a stationary and isotropic solid is given by [1]:

$$\nabla \cdot k(\vec{r})\nabla T(\vec{r}) + q'''(\vec{r}) = 0, \tag{5a}$$

with boundary condition

$$T(\vec{r}_s) = 0, \tag{5b}$$

where $k(\vec{r})$ is the thermal conductivity and $q'''(\vec{r})$ is the internal heat source.

If we compare Eq. (5) with Eq. (4), it is easily ascertained that Eq. (4) becomes Eq. (5) by setting

$$\Sigma_s(\vec{r}) = \frac{1}{3k(\vec{r})}, \tag{6}$$

and

$$S = q'''(\vec{r}), \tag{7}$$

with a large β and the problem domain extended by d .

The Monte Carlo method is extremely versatile in solving Eqs. (1), (2) and (3) with very complicated geometry and strong heterogeneity of the medium. Thus, Eq. (3) is solved by the Monte Carlo method (with a large β) to obtain $\phi(\vec{r})$. The result of $\phi(\vec{r})$ is then translated to provide $T(\vec{r}) = \phi(\vec{r}) - \phi(\vec{r}_s)$ as the solution of Eq. (5) [See Fig. 3.]

Here, $\beta > 1$ is a scaling factor rendering the transport phenomena diffusion-like. A large scaling factor plays an additional role of reducing the extrapolation distance to the order of a mean free path. To choose a proper value for β , we introduce an adjoint problem to perform sensitivity studies, specific results for a pebble problem provided later in this section.

Proof of principles of the method

In order to confirm or provide proof of principles of the Monte Carlo method described in Section 2.2, first we consider a simple heat conduction problem which allows analytic solution. The problem consists of one-dimensional slab geometry, isotropic solid, and uniformly distributed internal heat source under steady state. The left side has reflective boundary condition and the right side has zero temperature boundary condition. Fig. 4(a) shows the original problem and Fig. 4(b) shows the extended problem to be solved by the Monte Carlo method, incorporating the boundary layer correction. Table 1 provides the calculational conditions.

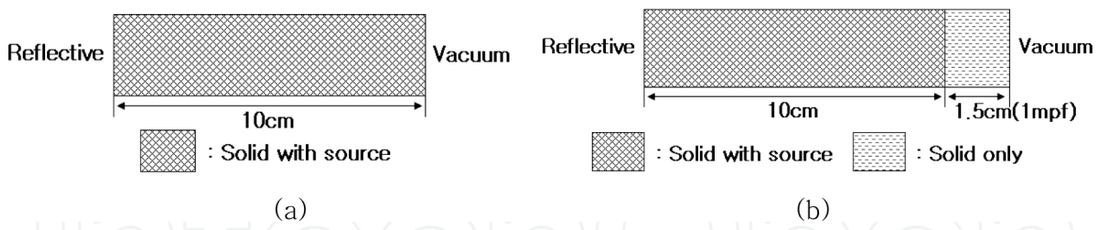

Fig. 4. A one-dimensional slab test problem

Thermal Conductivity ($W / cm \cdot °K$)	Internal Heat Source(W / cm^3)	Extrapolation Thickness (mfp)	Scaling Factor
0.5	0.01	1	1

Table 1. Calculation Conditions for Simple Problem

Figs. 5 and 6 show the Monte Carlo method results with and without the extension by extrapolation thickness in comparison with the analytic solution. Note that the result of the Monte Carlo method with boundary layer correction is in excellent agreement with the analytic solution.

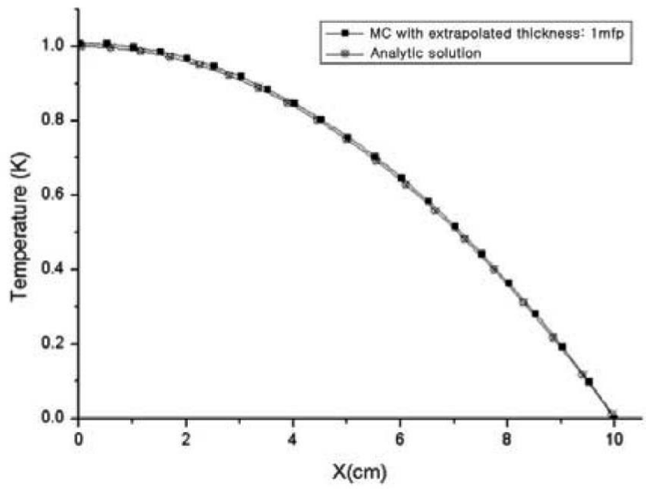

Fig. 5. Monte Carlo heat conduction solution with extrapolated layer

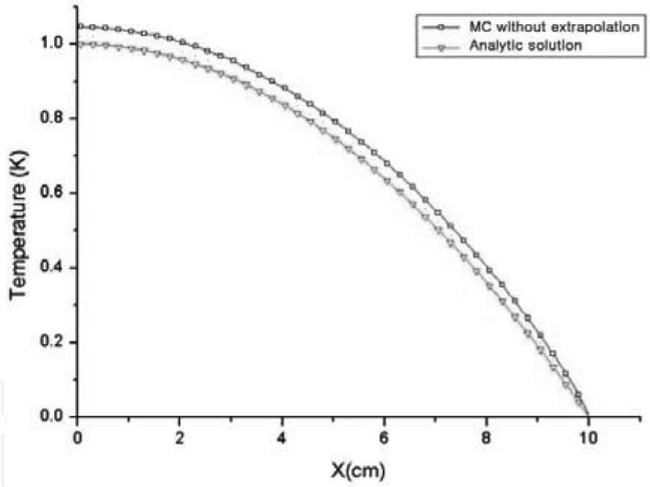

Fig. 6. Monte Carlo heat conduction solution without extrapolated layer

To test the method on a realistic problem, the FLS (Fine Lattice Stochastic) model and CLCS (Coarse Lattice with Centered Sphere) model [14] for the random distribution of fuel particles in a pebble are used to obtain the heat conduction solution by the Monte Carlo method. Details of this process are described in Table 2 and Fig. 7. The power distribution generated in a pebble is assumed uniform within a kernel and across the particle fuels. The pebble is surrounded by helium at 1173K with the convective heat transfer coefficient h=0.1006($W / cm^2 \cdot °K$). A Monte Carlo program HEATON [15] was written to solve heat conduction problems using the MCNP5 code as the major computational engine.

Material	Kernel	Buffer	Inner PyC	SiC
Thermal Conductivity $(W/cm\cdot°K)$	0.0346	0.0100	0.0400	0.1830
Radius (cm)	0.02510	0.03425	0.03824	0.04177

Material	Outer PyC	Graphite-matrix	Graphite-shell
Thermal Conductivity $(W/cm\cdot°K)$	0.0400	0.2500	0.2500
Radius (cm)	0.04576	2.5000	3.0000

Number of Triso Particles	9394
Power/pebble (W)	1893.95

Table 2. Problem Description for a Pebble

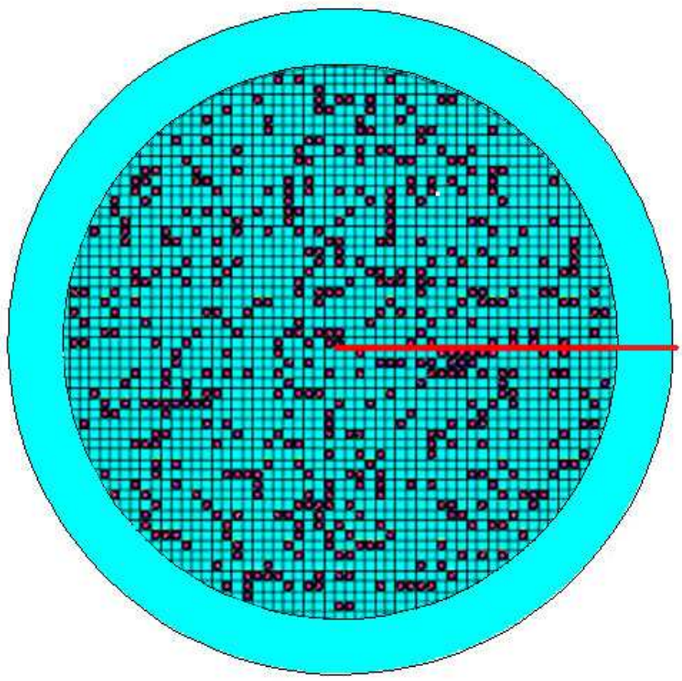

Fig. 7. A planar view of a particle random distribution for a pebble problem with the FLS model

Heat conduction solutions for the pebble problem with the data in Table 2 using the Monte Carlo method are shown in Table 3 and Fig. 8. The number of histories used was 10^7. Parallel computation with 60 CPUs (3.2GHz) was used. When the scaling factor β increases, the solution of the pebble problem approaches its asymptotic solution (diffusion solution). However, the computational time increases rapidly as the scaling factor increases. In Table 3 and Fig. 8, it is shown that a scaling factor of 10 or 20 is not large enough.

Scaling Factor	Maximum Temp. ($°K$)	Relative Error[a] (%)	Graphite Temp. Near Center($°K$)	Relative Error[a] (%)	Computing Time (sec)	Translation Temp. ($°K$)
1	1674.21	1.59	158.33	0.71	534	27.08
10	1556.96	1.14	1533.53	0.34	6,692	2.72
20	1558.54	1.12	1531.67	0.30	20,297	1.36
50	1553.22	1.11	1527.07	0.28	99,454	0.54

[a] One standard deviation in temperature / mean estimate of temperature by Monte Carlo ×100%

Table 3. Results of Fig. 7 Problem

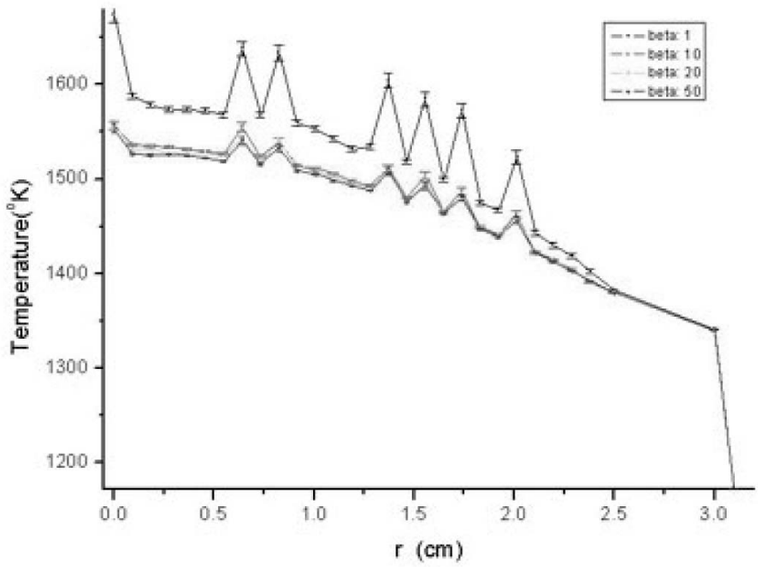

Fig. 8. Results along the red line of Fig. 7 vs the scaling factor

Therefore, it is necessary to determine an effective scaling factor that renders the problem more diffusive. This can be done using an adjoint calculation. Using an adjoint calculation, the computing time is reduced as the calculation transports particles backward from the detector region (at the center of the pebble) to the source region. Additionally, it is possible that the changed tally regions used in the adjoint calculation allow effective particle tallies.

Scaling Factor	Maximum Temp. ($°K$)	Standard Deviation($°K$)	Computing Time (sec)
1	1685.131	0.409	47
20	1558.817	0.308	1,427
50	1553.931	0.304	7,298
80	1553.586	0.304	17,976
100	1552.995	0.303	27,240
120	1552.713	0.303	39,435

Table 4. Maximum Temperature and Computing Time for Fig. 9

In order to confirm the appropriate scaling factor, the problem with the data of Table 2 and in Fig. 7 was again tested with a smaller number (10^6) of histories compared to the number used in the forward calculation. The results depending on the scaling factor are shown in Fig. 9 and Table 4.
Fig. 9 shows that the center temperature of a fuel pebble approaches its asymptotic solution (diffusion solution) as the scaling factor increases. Therefore, to obtain a diffusion solution, a scaling factor of > 30 (e.g., 50) is required.

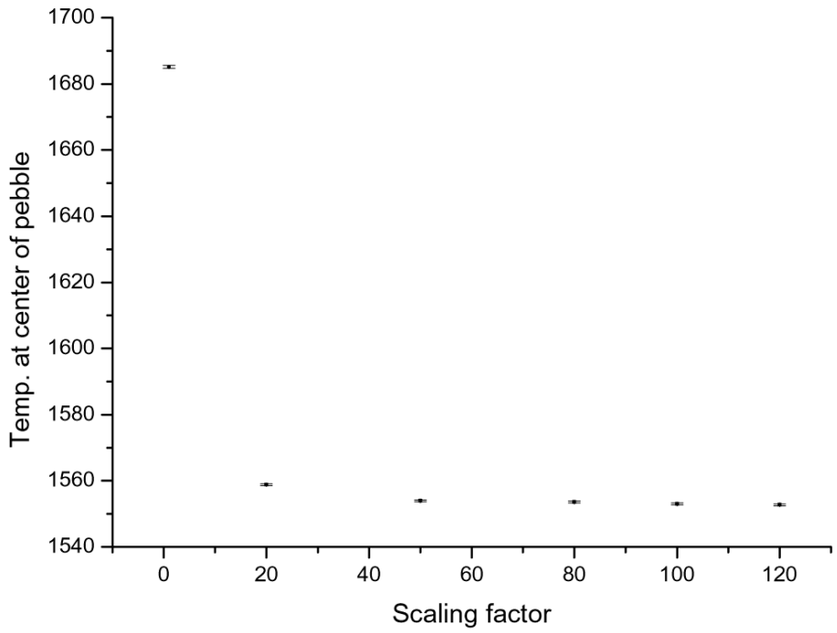

Fig. 9. Center temperature by the adjoint calculation

2.3 Heat conduction problems

Given varying-temperature boundary condition

The first kind of the boundary conditions is the prescribed surface temperature:

$$T(\vec{r}_s) = f(\vec{r}_s), \tag{8}$$

where $\vec{r}_s$ is on a boundary surface. Since the paradigm heat conduction problem that the Monte Carlo method can treat is a problem with zero temperature boundary condition (as described in Section 2.2), let T be decomposed into T^* and $\tilde{T}$ as follows:

$$T(\vec{r}) = T^*(\vec{r}) + \tilde{T}(\vec{r}), \tag{9}$$

where T^* satisfies the zero boundary condition, and $\tilde{T}$ is chosen such that it satisfies the given boundary condition (8). Eq. (5a) can then be rewritten as:

$$-\nabla \cdot k(\vec{r})\nabla T(\vec{r}) = -\nabla \cdot k(\vec{r})\nabla(T^* + \tilde{T}) = q'''(\vec{r}), \tag{10}$$

or

$$-\nabla \cdot k(\vec{r})\nabla T^{*}(\vec{r}) = q^{*'''}(\vec{r}), \tag{11a}$$

where the new source $q^{*'''}(\vec{r})$ is defined by

$$q^{*'''}(\vec{r}) = \nabla \cdot k(\vec{r})\nabla \tilde{T}(\vec{r}) + q'''(\vec{r}), \tag{11b}$$

Eq. (11a) is to be solved for T^{*} by the Monte Carlo method [6-8]. The Monte Carlo method cannot deal easily with the gradient term, $\nabla \cdot k(\vec{r})\nabla \tilde{T}$, in Eq. (11b) when the boundary condition temperature is not a constant and $k(\vec{r})$ is not smooth enough. In order to evaluate the new source term as simply as possible, let $\tilde{T}$ be zero in internally complicated thermal conductivity region as shown in Fig. 10. In addition, $\tilde{T}$ and $\nabla \tilde{T}$ must be continuous in the whole problem domain to render the $\nabla \cdot k(\vec{r})\nabla \tilde{T}$ term treatable.

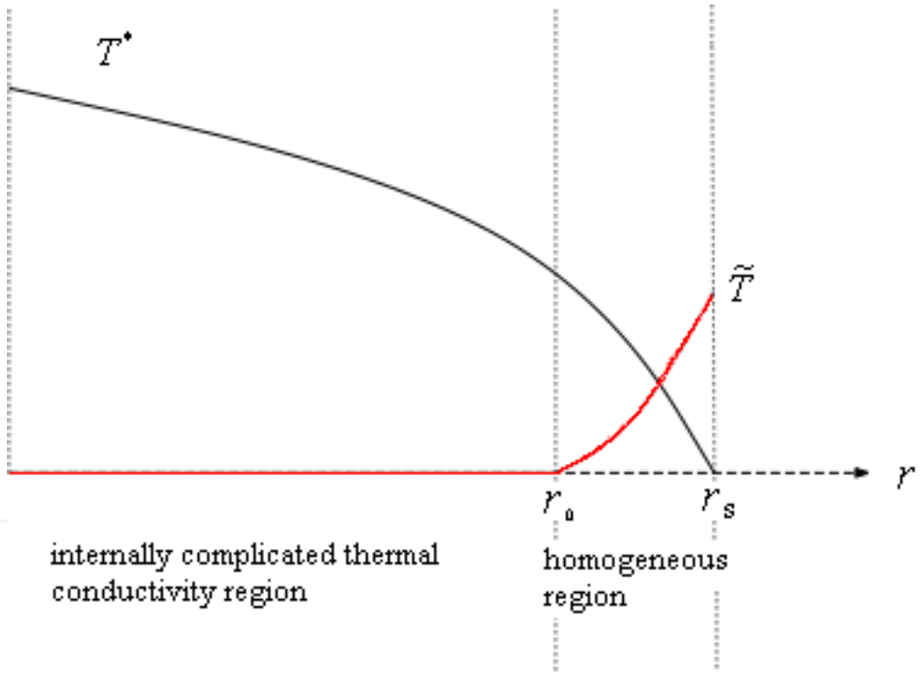

Fig. 10. Solution Decomposition $T = T^{*} + \tilde{T}$,

In Ref. [8], the following $\tilde{T}$ is chosen for a three-dimensional spherical model:

$$\tilde{T} = U(r) f(r_s, \theta, \omega) \frac{(r - r_0)^2}{(r_s - r_0)^2}, \tag{12}$$

where $f(r_s, \theta, \omega)$ is the given boundary condition (8), θ and ω indicate polar and azimuthal angle, respectively. r_s is radius to the boundary surface and there may be internally complicated thermal conductivity region inside r_0.

Convection boundary condition

A convection boundary condition is usually given by

$$k_1 \frac{\partial T(\vec{r}_s)}{\partial n} = h(T_b - T(\vec{r}_s)), \tag{13}$$

where k_1 is the thermal conductivity of medium 1 (solid), h and T_b are the convective heat transfer coefficient and the bulk temperature of the convective medium, respectively. This condition can be equivalently transformed to a given temperature (T_b) boundary condition of a related problem, in which the convective medium is replaced by a hypothetical conduction medium with thermal conductivity

$$k_2 = h\Delta n \left(\frac{r_s}{r_b} \right), \tag{14}$$

where Δn is additional thickness beyond $r_s (\Delta n = r_b - r_s)$ in a spherical geometry. Here r_b is the radius where T_b occurs. k_2 involves a geometry factor and k_2 's for several geometries are shown in Table 5 (see Appendix B for the derivation).

Geometry	k_2
Sphere	$h(r_b - r_s)\left(\frac{r_s}{r_b} \right)$
Cylinder	$hr_s ln\left(\frac{r_b}{r_s} \right)$
Slab	$h(x_b - x_s)$

Table 5. k_2 for Several Geometries

There is no approximation in the k_2 expressions for given h if there is no heat source in the fluid. The transformed problem can then be solved by the Monte Carlo method in Section 2.1 with replacement of r_0 by r_s and r_s by r_b, and T_b as the boundary condition. Eq. (13) with the right-hand side replaced by Eq. (14) is no more than a continuity expression of heat flux on the interface. Fig. 11 shows the concept in this transformation.

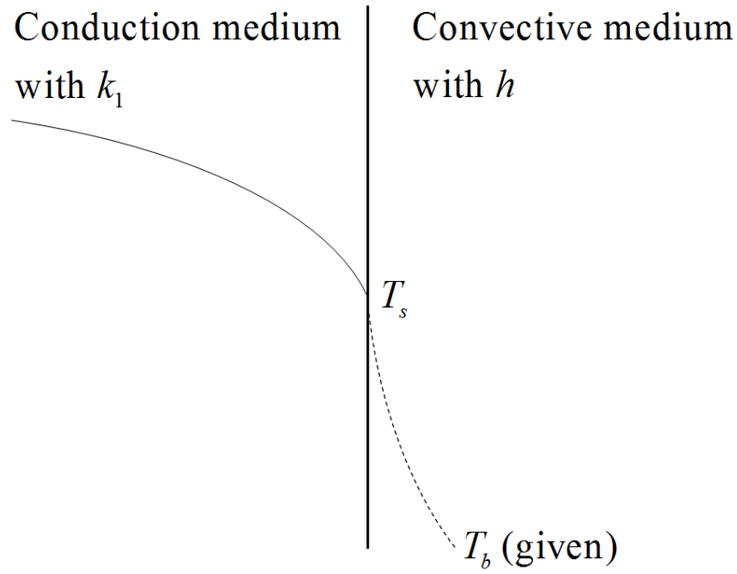

(a) Original problem

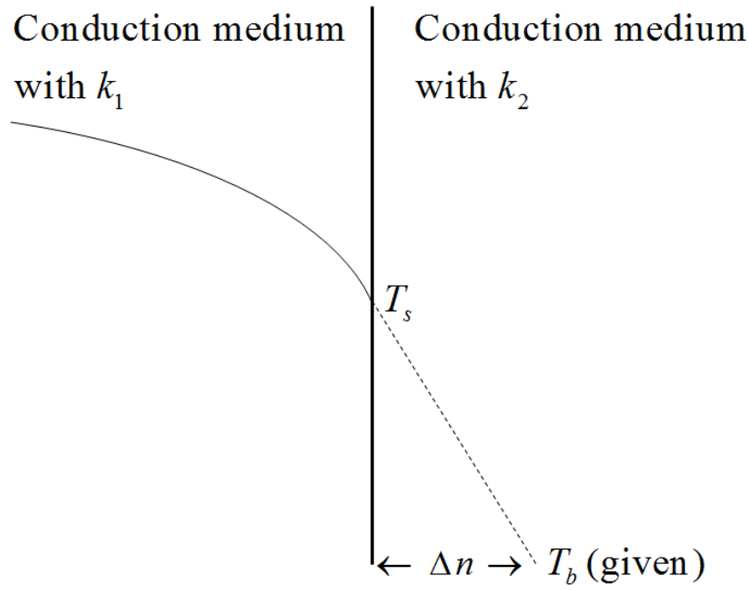

(b) Equivalent problem

Fig. 11. Transformation of a convective medium to an equivalent conduction medium preserving heat flux

Examples

The method is applied to a pebble fuel with Coarse Lattice with Centered Sphere (CLCS) distribution of fuel particle [14]. The description of a pebble fuel is shown in Fig. 12 and Table 2. The pebble fuel is surrounded by helium at given bulk temperature with convective heat transfer coefficient $h = 0.1006(W / cm^2 \cdot °K)$. The number of histories used in the Monte Carlo calculation was 10^7.

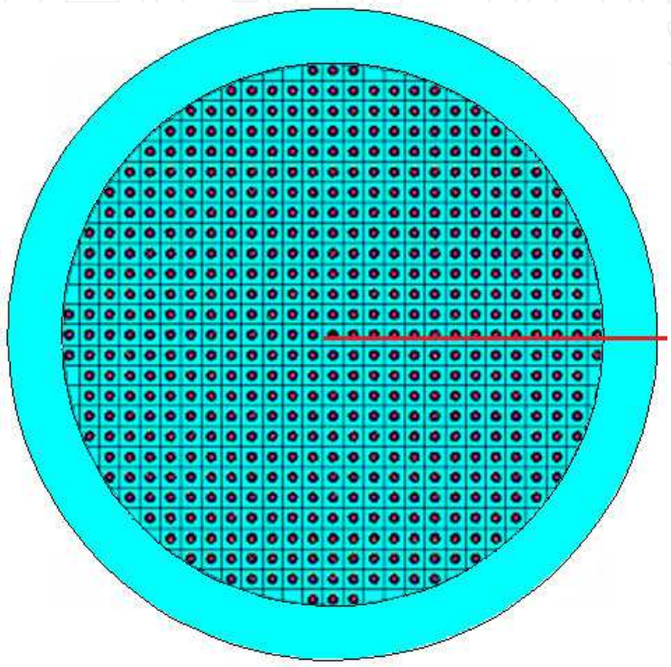

Fig. 12. CLCS distribution

Test Problem 1 is defined by the following non-constant bulk temperature of the helium coolant:

$$1173 + 10(1 + cos\,\theta)°K, \tag{15a}$$

where θ is the polar angle, or equivalently

$$1173 + 10\left(1 + \frac{z}{\sqrt{x^2 + y^2 + z^2}}\right), \tag{15b}$$

where

$$x^2 + y^2 + z^2 = r_b^2, \tag{15c}$$

with $r_b = 3.1$, x, y and z in centimeters.

The results are shown in Figs. 13, 14 and 15.

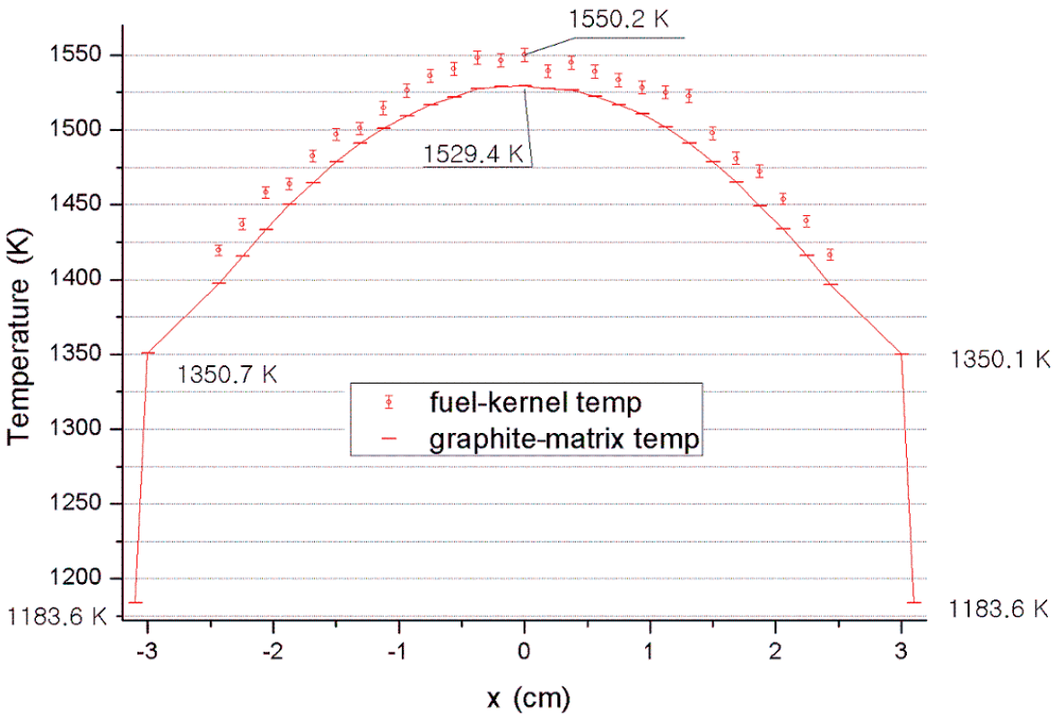

Fig. 13. Temperature distribution along x -direction with $y = z = 0$ in Test Problem 1

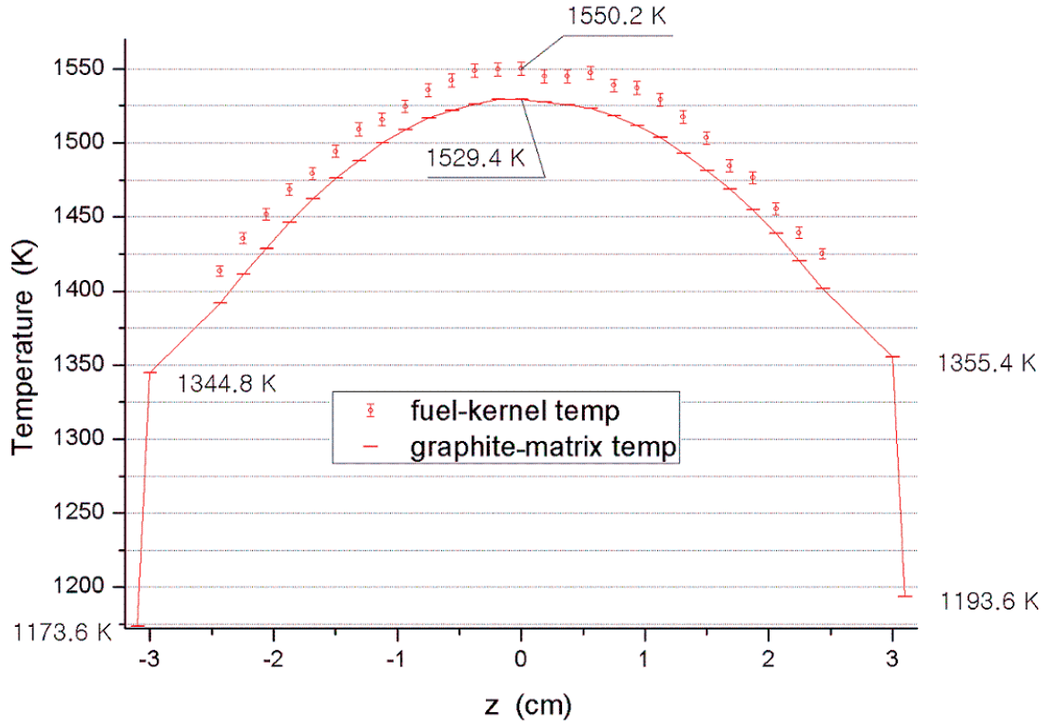

Fig. 14. Temperature distribution along z -direction with $x = y = 0$ in Test Problem 1

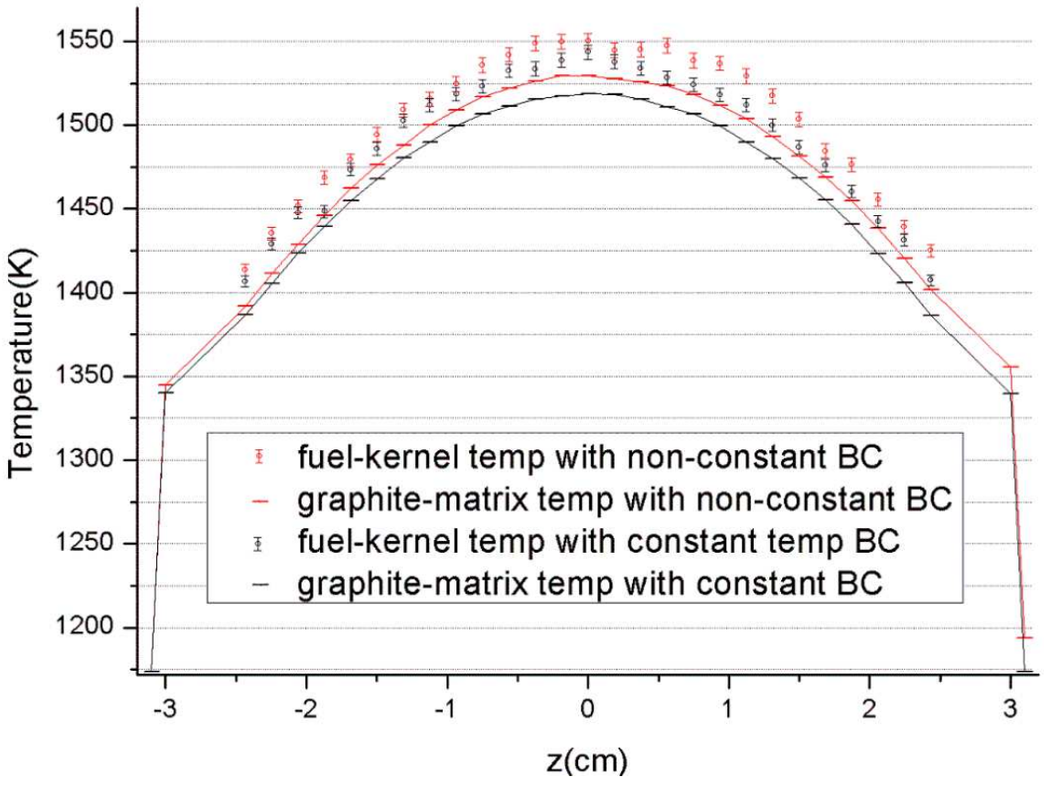

Fig. 15. Comparison of Test Problem 1 and a problem with constant helium bulk temperature ($1173\,°K$)

Test Problem 2 is defined by the following non-constant bulk temperature of the helium coolant:

$$1173 + 10 + (x + y + z)°K \tag{16a}$$

where

$$x^2 + y^2 + z^2 = r_b^2, \tag{16b}$$

with $r_b = 3.1$, x, y and z in centimeters.

The results are shown in Figs. 16, 17, and 18.

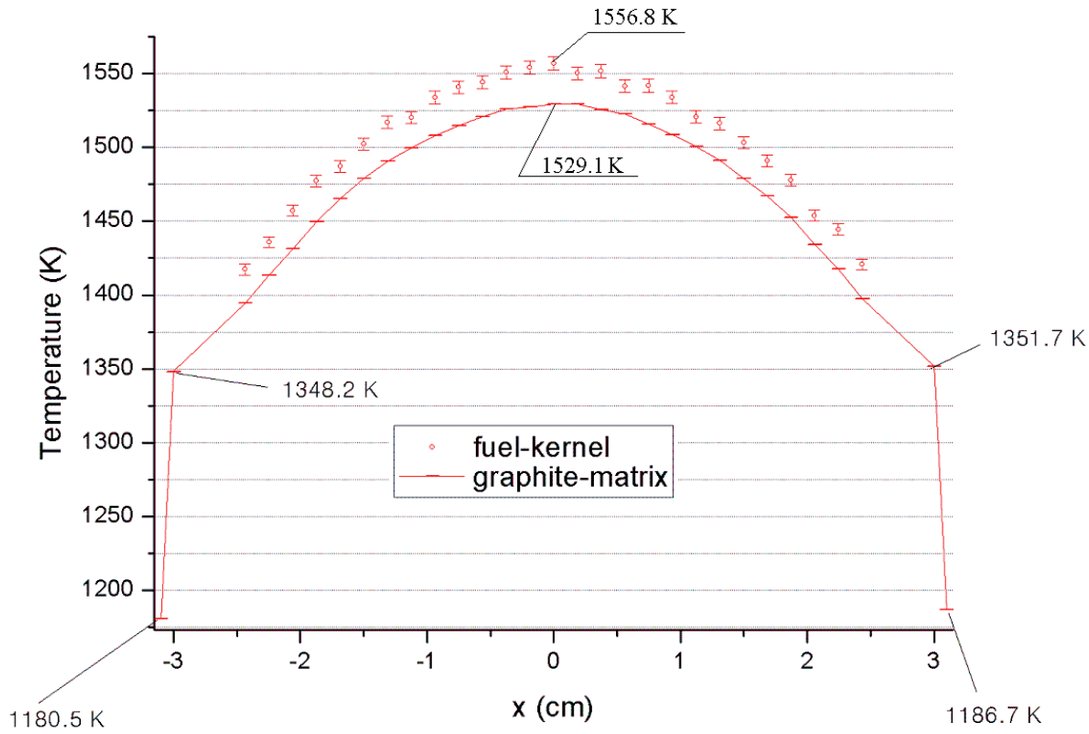

Fig. 16. Temperature distribution along x -direction with $y = z = 0$ in Test Problem 2

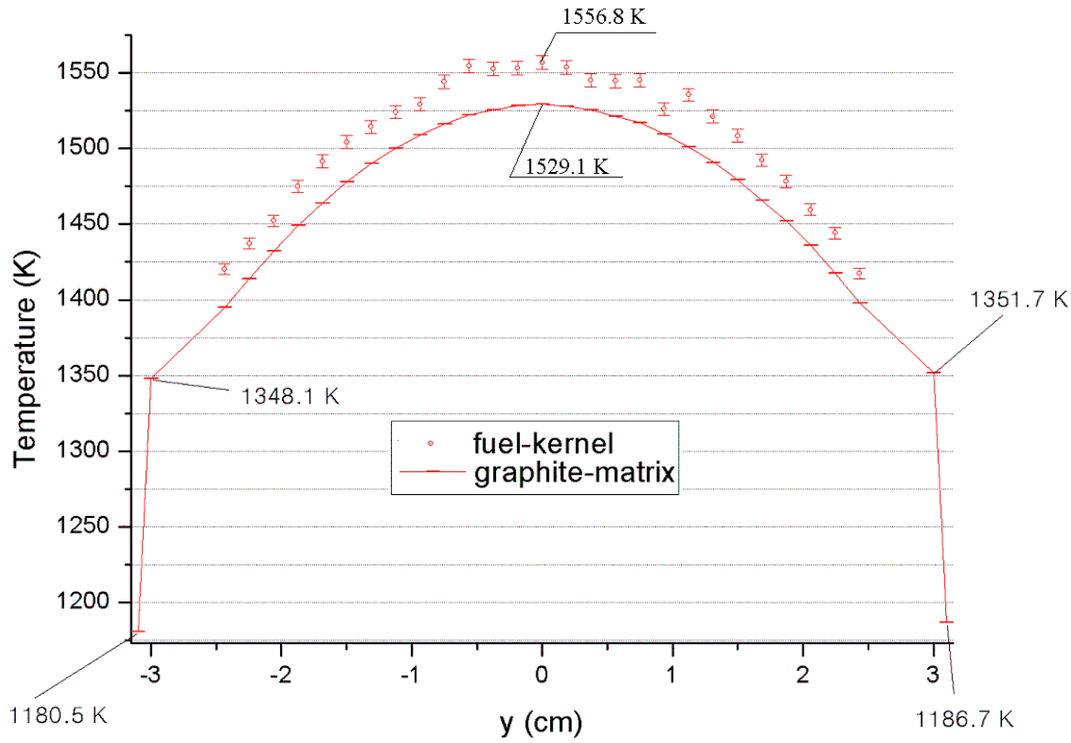

Fig. 17. Temperature distribution along z -direction with $x = y = 0$ in Test Problem 2

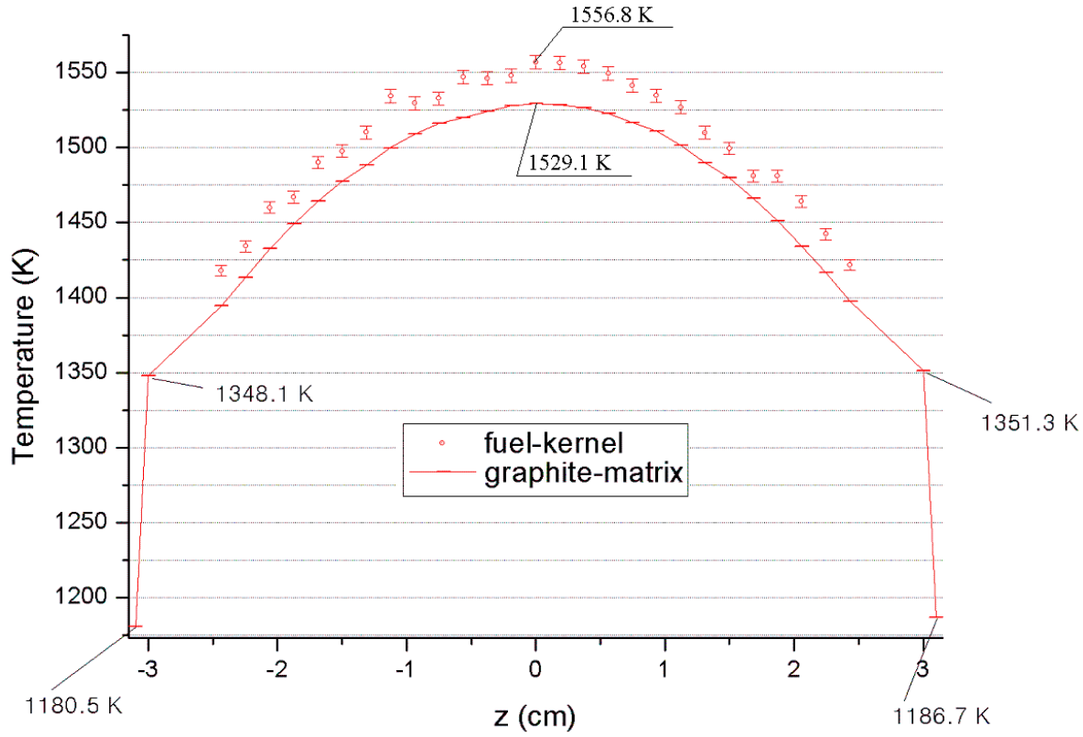

Fig. 18. Temperature distribution along y -direction with $x = z = 0$ in Test Problem 2

3. Applications

3.1 Comparison between the FLS (Fine Lattice Stochastic) model and analytic bound solutions

In this section, the data of the geometry information and thermal conductivity are identical to those in Table 2. Based on the results in the previous section, temperature distributions were calculated using a scaling factor of 50. Three triso particle configurations obtained by randomly distributed fuels in a pebble were considered (using the FLS model in Ref. 14). The tally regions as shown in Fig. 19 were chosen. If a (fine) lattice has a heat source, the tally is done over the kernel volume. If the lattice consists of only graphite, tally is done over the lattice cubical volume.

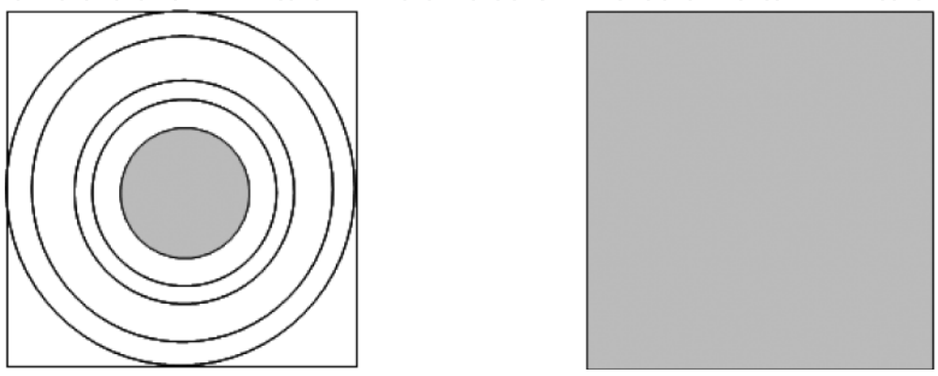

Fig. 19. Tally regions with and without a heat source

Fig. 20 shows the temperature distributions obtained from the Monte Carlo method compared to the two analytic bound solutions superimposed with a particle located at the center of the pebble based on commonly quoted homogenized models [16]. It is important to note that the volumetric analytic solution usually presented in the literature [17] predicts lower temperatures than those of
(thus underestimates) the Monte Carlo results. In the Monte Carlo results, the fuel-kernel temperature and graphite-matrix temperature are distinctly calculated. The results are summarized in Table 6.

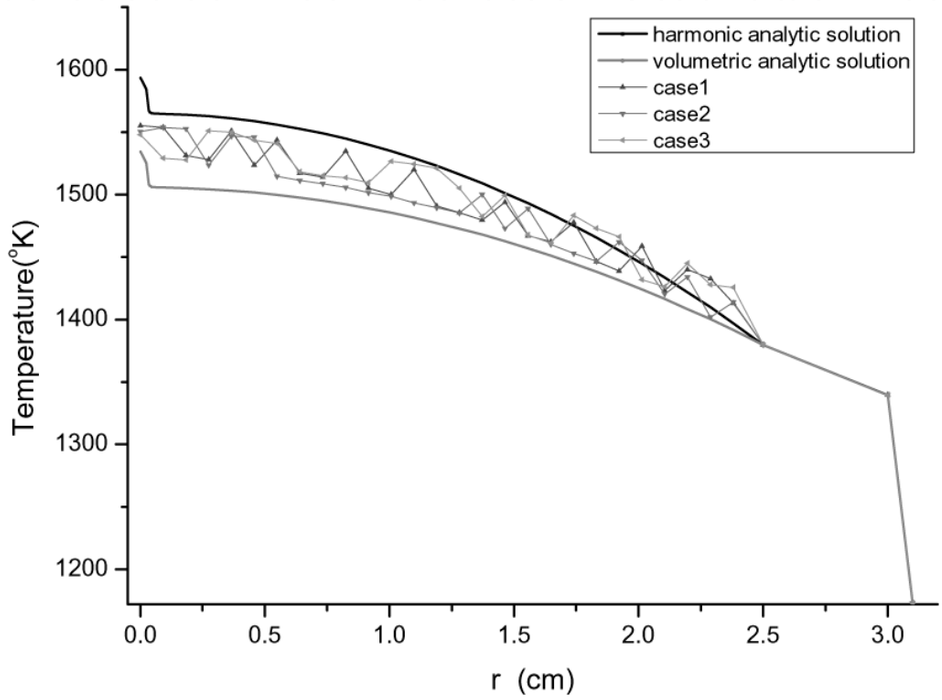

Fig. 20. Temperature profiles depending on the triso particle distribution configuration compared to two homogenized models

	Max. Temp. ($°K$)	Average Kernel Temp. ($°K$)	Average Graphite Temp. ($°K$)
Case 1	1555.07	1497.84	1487.61
Case 2	1553.77	1499.63	1480.43
Case 3	1550.87	1501.89	1489.38
Average	1553.23	1499.79	1485.80

Table 6. Maximum, Average Kernel and Graphite Temperatures from Fig. 20

For a fourth triso particle configuration (Case 4), the tally region was further refined as shown in Fig. 21 to provide more accurate graphite-moderator temperature. Essentially, if the lattice has a kernel (heat source), the tally is done over the kernel volume and over the moderator (graphite and layers) volume separately. Otherwise, if the lattice consists of only graphite, the tally is done over the cubical volume.

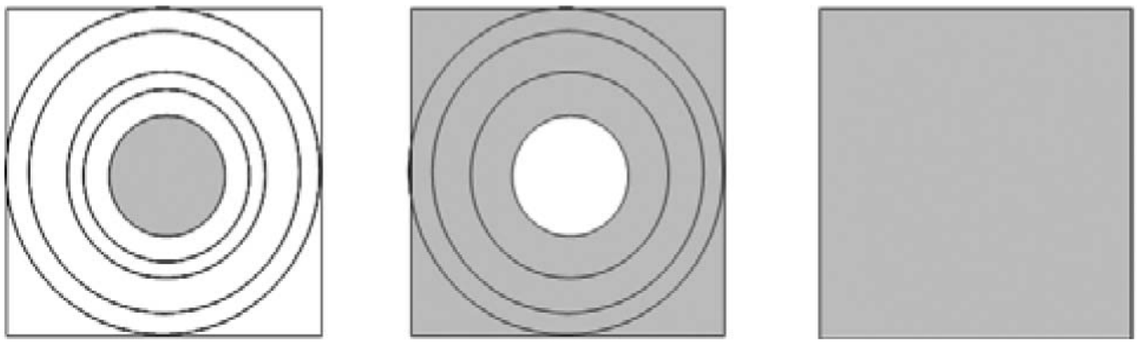

Fig. 21. Tally regions depending on the geometries

In this problem, geometry information is identical to those shown in Table 2. The distributed particle configuration is shown in Fig. 22. The kernel and graphite-moderator temperatures are shown in Fig. 23 and Table 7.

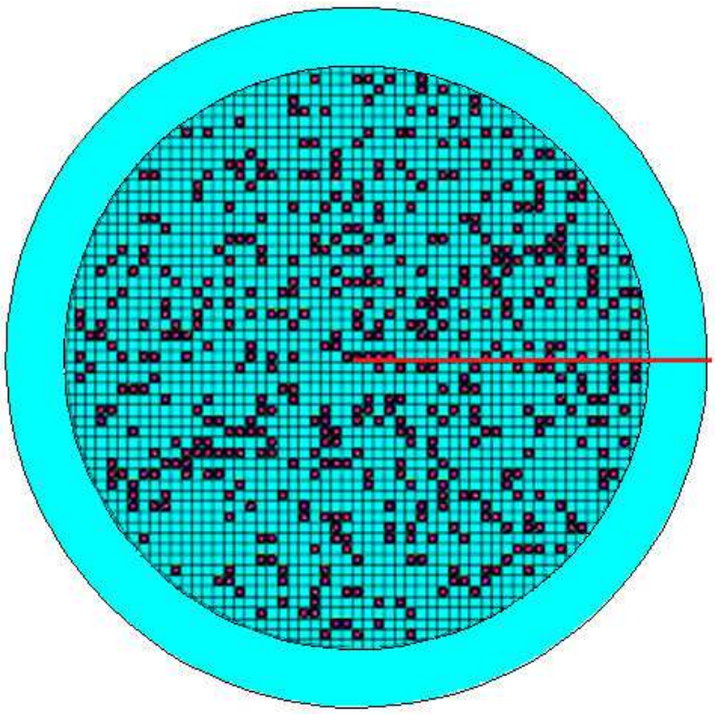

Fig. 22. A planar view of a fourth particle distribution configuration with the FLS model

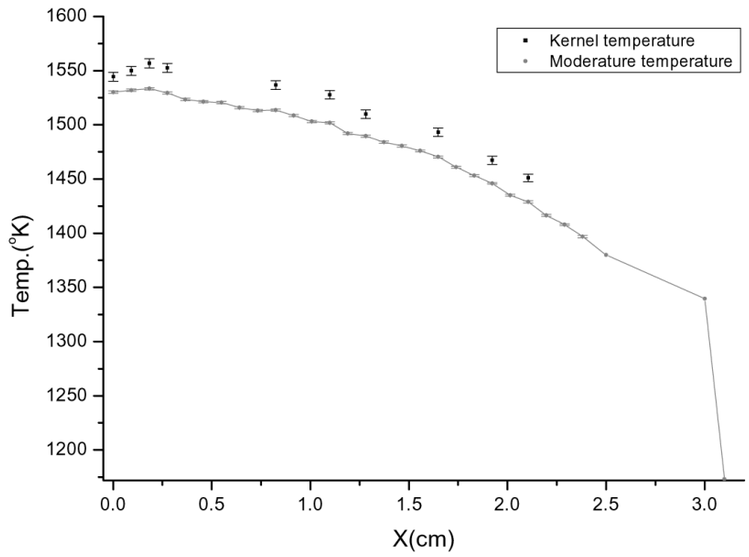

Fig. 23. Temperature distribution along red line for Fig. 22

Maximum temperature ($°K$)	1556.70
Averaged kernel temperature ($°K$)	1518.88
Averaged moderator temperature ($°K$)	1484.61
Surface temperature at 2.5cm ($°K$)	1379.82
Surface temperature at 3.0cm ($°K$)	1339.65
Computing time	43h 35m 9s

Table 7. Results for the Fourth Configuration Shown in Fig. 23

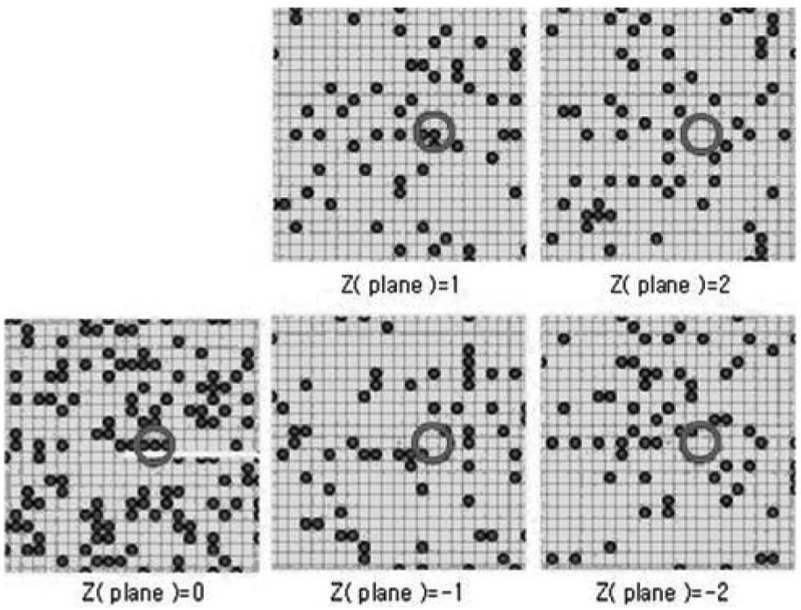

Fig. 24. Cross-sectional views for Fig. 22

The temperature profile on the $z = 0$ plane along red line is shown in Fig. 23 and Table 7. In this FLS model, the maximum fuel temperature appears not at the center point but near the central region, as the fuels are concentrated on the right side of the center point on the $z = 0$ plane, as shown in Fig. 24. Note that the red circle in Fig. 24 denotes particles with the dominant effect of the temperature increase on the $z = 0$ plane.

3.2 CLCS (Coarse Lattice with Centered Sphere) model

The temperature distribution was obtained again for the CLCS (Coarse Lattice with Centered Sphere) model [14]. In this model, the tally regions used are shown in Fig. 25. The general geometry
information is identical to that in Table 2, except that there are 9315 triso particles and each triso particle takes one lattice cube (and vice versa), as shown in Fig. 26. The resulting temperature distribution for the CLCS model is shown in Fig. 27.

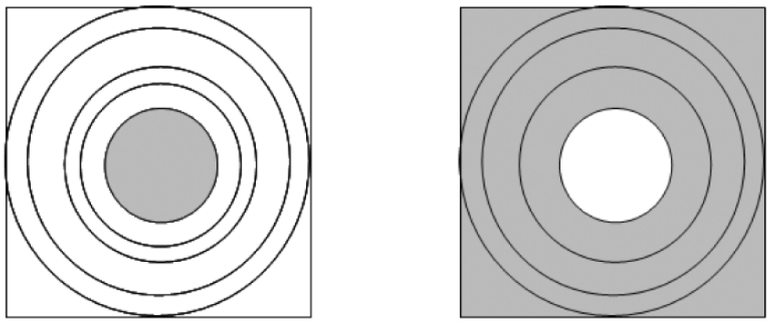

Fig. 25. Tally regions for the CLCS model

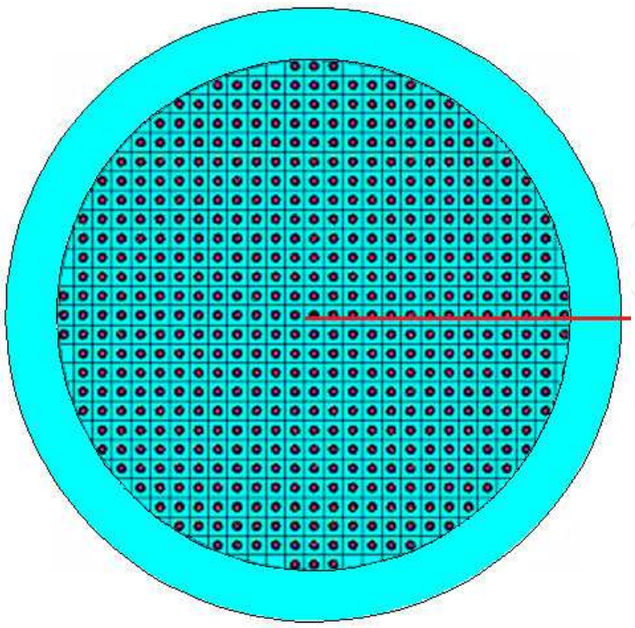

Fig. 26. Fuel particle configuration for the CLCS model

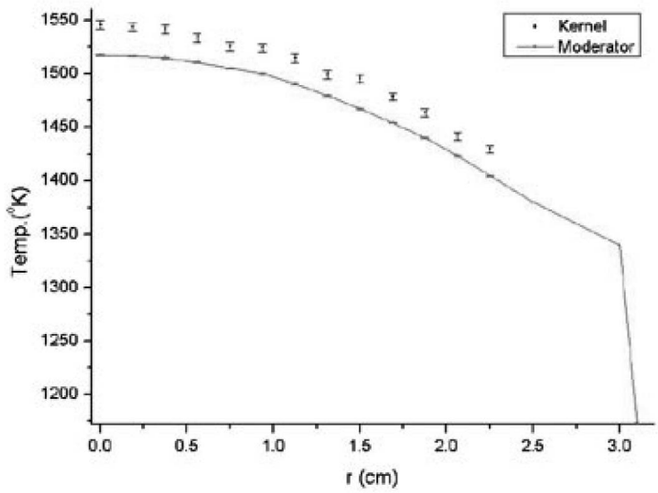

Fig. 27. Results of cubes along red line for Fig. 26

4. Concluding remarks

A Monte Carlo method for heat conduction problems was presented in this chapter. Based on the asymptotic theory correspondence between neutron transport and diffusion equations, it is shown that the particle transport Monte Carlo simulation can provide solutions to the heat conduction problems with two modeling devices introduced: i) boundary layer correction by the extended problem domain and ii) scaling factor to increase the diffusivity of the problem.

The Monte Carlo method can be used to solve heat conduction problems with complicated geometry (e.g. due to the extreme heterogeneity of a fuel pebble in a VHTGR, which houses many thousands of coated fuel particles randomly distributed in graphite matrix). It can handle typical boundary conditions, including non-constant temperature boundary condition and heat convection boundary condition. The HEATON code was written using MCNP as the major engine to solve these types of heat conduction problems. Monte Carlo results for randomly sampled configurations of triso fuel particles were presented, showing the fuel kernel temperatures and graphite matrix temperatures distinctly. The fuel kernel temperatures can be used for more accurate neutronics calculations in nuclear reactor design, such as incorporating the Doppler feedback. It was found that the volumetric analytic solution commonly used in the literature predicts lower temperatures than those of the Monte Carlo results. Therefore, it will lead to inaccurate prediction of the fuel temperature under Doppler feedback, which will have important safety implications.

An obvious area of further application is the time transient problem. The results of the steady-state heterogeneous calculations by Monte Carlo (as described in this chapter) can be used to construct a two-temperature homogenized model that is then used in transient analysis [18].

While the Monte Carlo method has its capability and efficacy of handling heat conduction problems with very complicated geometries, the method has its own shortcomings of the long computing time and variance due to the statistical results. It also has a limitation in that it provides temperatures at specific points rather than at the entire temperature field.

Appendix A: Elements of Monte Carlo method

A.1 Introduction

In a typical form of the particle transport Monte Carlo method [9,19], we simulate particle (e.g., neutron) behavior by following a finite number, say *N*, of particle histories and tallying the appropriate events needed to calculate the quantity of interest. The simulation is performed according to the physical events (expressed by each term in the transport equation) that a particle would encounter through the use of random numbers. These random numbers are usually generated by a pseudo random number generator, that provides uniform random number ξ between 0 and 1. In each particle history, the random numbers are generated and used to sample discrete events or continuous variables as the case may be according to the probability distribution functions. The results of tally are processed to provide estimates for the mean and variance of the quantity of interest, e.g., neutron flux, current, reaction rate, or some other quantities.

A.2 Basic operations of sampling

A.2.1 Sampling of random events

The discrete events such as the type of nuclides and collisions are simple to sample. For example, suppose that there are in the medium I nuclides with total macroscopic cross sections, $\Sigma_t^{(i)}$, $i = 1,2,\cdots,I$. Let

$$\Sigma_t = \sum_{i=1}^{I} \Sigma_t^{(i)} , \tag{A1}$$

and

$$P_i = \frac{\Sigma_t^{(i)}}{\Sigma_t}, \quad i = 1,2,\cdots,I. \tag{A2}$$

Now draw a random number ξ and if

$$P_1 + P_2 + \cdots + P_{i-1} \le \xi < P_1 + P_2 + \cdots + P_i, \tag{A3}$$

then the i -th nuclide is selected and the neutron collides with nuclide i . After determination of the nuclide, the type of collisions (absorption, fission, or scattering, etc.) is determined in a similar way. If the event is scattering, the energy and direction of the scattered neutron are sampled. In addition, the distance a neutron travels before suffering its next collision is sampled. These values are continuous variables and thus determined by sampling according to the appropriate probability density function $f(x)$. For example, the distance l to next collision (within the same medium) is distributed as

$$f(l)dl = e^{-\Sigma_t l}\Sigma_t dl , \tag{A4}$$

with its cumulative distribution function

$$F(l) = \int_0^l f(l')dl' = 1 - e^{-\Sigma_t l} . \tag{A5}$$

Since $F(l)$ is uniformly distributed between 0 and 1, we draw a random number ξ and let

$$F(l) = \xi \,, \tag{A6}$$

that in turn provides

$$l = -\frac{ln(1-\xi)}{\Sigma_t} = -\frac{ln(\xi)}{\Sigma_t} \,. \tag{A7}$$

A.2.2 Geometry tracking

In typical Monte Carlo codes, the geometries of the problem are created with intersection and union of surfaces. In turn, the surfaces are defined by a collection of elementary mathematical functions. For example, the geometry in Fig. A1 would be defined by functions that represent four straight lines and a circle.

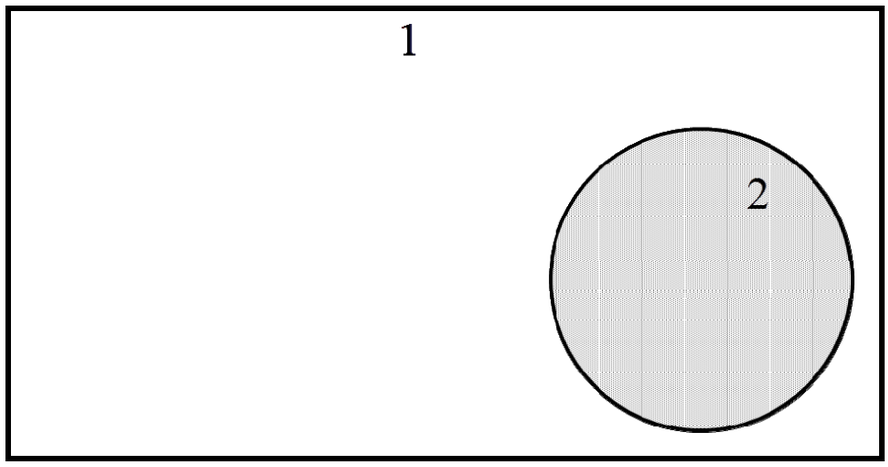

Fig. A1. An example of problem geometry with two material media

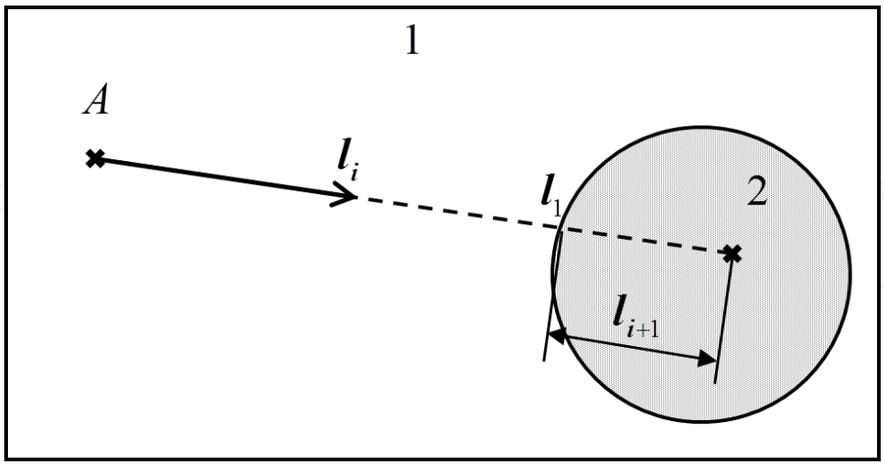

Fig. A2. Geometry tracking

Suppose that the neutron we follow is now at point A and heading to the direction as in Fig. A2. In order to determine next collision point, first we calculate the distance (l_1) to the nearest material interface and draw a random number ξ_i, then two cases occur; i)

if $\xi_i \geq e^{-\Sigma_{t1} l_1}$, the collision is in region 1 at point $l_i = -\ln \xi_i / \Sigma_{t1}$, or ii) if $\xi_i < e^{-\Sigma_{t1} l_1}$, it says that the collision is beyond region 1, so draw another random number ξ_{i+1} to determine the collision point that may be in region 2 at $l_{i+1} = -\ln \xi_{i+1} / \Sigma_{t2}$ beyond l_1 along the same direction. This process continues until the neutron is absorbed or leaks out of the problem boundary.

A.2.3 Tally of events

To calculate neutron flux of a region, current through a surface, or reaction rate in a region, the events that are usually tallied are i) number of collisions, ii) total track length traveled, or iii) number of crossings through a surface. For example, suppose that we like to calculate average scalar flux $\bar{\phi}$ in a volume element V with total cross section Σ_t. From a well-known relation,

$$\bar{c} = V \Sigma_t \bar{\phi} , \tag{A8}$$

where c is the number of collisions made by neutrons in V, we can calculate $\bar{\phi}$ by tallying the number of collisions:

$$\bar{\phi} = \frac{1}{V \Sigma_t} \bar{c} . \tag{A9}$$

We provide sample estimate of $\bar{c}$ by

$$\hat{c} = \frac{1}{N} \sum_{n=1}^{N} c_n , \tag{A10}$$

where c_n is the number of collisions made in V during the n-th history and N is a large number. In addition, we also provide sample estimate of variance on c by

$$\begin{aligned} S^2 &= \frac{1}{N-1} \sum_{n=1}^{N} (c_n - \hat{c})^2 \\ &= \frac{N}{N-1} \sum_{n=1}^{N} (\widehat{c^2} - \hat{c}^2), \end{aligned} \tag{A11}$$

where

$$\widehat{c^2} = \frac{1}{N} \sum_{n=1}^{N} s_n^2 . \tag{A12}$$

It can be easily shown that the sample standard deviation on $\hat{c}$ is

$$\sigma_{\hat{c}} = \frac{S}{\sqrt{N}} , \tag{A13}$$

which suggests to use a large N for accurate $\hat{c}$, since $\sigma_{\hat{c}}$ is a measure of uncertainty in the estimated $\hat{c}$.

Fig. A3 shows an example for c_n; in the shaded region,

$$c_1 = 0, c_2 = 1, c_3 = 1, and\, c_4 = 3,$$

thus

$$\hat{c} = \frac{1}{4} \times 5 = 1.25,$$

$$S^2 = \frac{3}{4} \times (\frac{11}{4} - 1.25^2) = 1.583,$$

$$\sigma_{\hat{c}} = \frac{\sqrt{1.583}}{\sqrt{4}} = 0.6291.$$

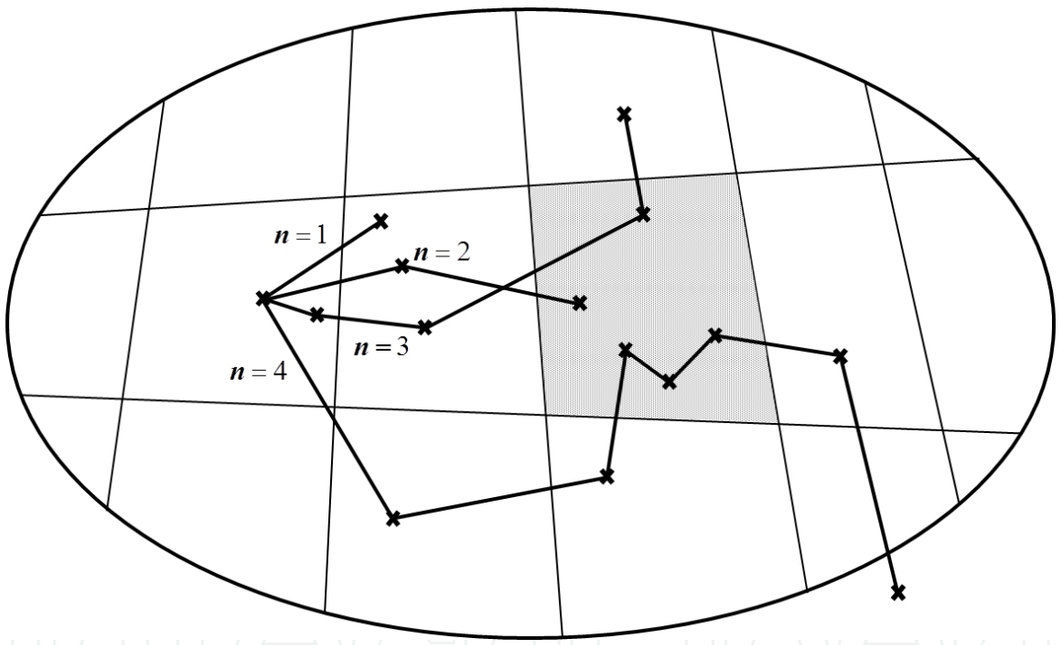

Fig. A3. Tally of number of collisions

Appendix B: Derivation of equivalent thermal conductivities

The expressions of k_2 (equivalent thermal conductivity) for the convective medium are derived in this Appendix for three (sphere, cylinder, slab) geometries.

B.1 Sphere geometry

The heat conduction equation in spherical coordinates is, in a region free of heat source,

$$\frac{k_2}{r^2} \frac{d}{dr} r^2 \frac{dT}{dr} = 0. \tag{B1}$$

Thus,

$$r^2 \frac{dT}{dr} = c_1, \tag{B2}$$

$$\frac{dT}{dr} = \frac{c_1}{r^2}, \tag{B3}$$

$$T = -\frac{c_1}{r} + c_2. \tag{B4}$$

From Eq. (B4),

$$T_s - T_b = c_1 \left(\frac{1}{r_b} - \frac{1}{r_s} \right) = c_1 \frac{r_s - r_b}{r_s r_b}, \tag{B5}$$

and thus

$$c_1 = \frac{r_s r_b}{r_s - r_b} (T_s - T_b), \tag{B6}$$

The convective boundary condition equation for spherical geometry is,

$$-k_2 \left. \frac{dT}{dr} \right|_{r_s} = h(T_s - T_b). \tag{B7}$$

Substituting Eqs. (B3) and (B6) into (B7), we have

$$k_2 = h(r_b - r_s) \left(\frac{r_s}{r_b} \right). \tag{B8}$$

B.2 Cylinder geometry

The heat conduction equation in cylindrical coordinates is, in a region free of heat source,

$$\frac{k_2}{r} \frac{d}{dr} r \frac{dT}{dr} = 0. \tag{B9}$$

Thus,

$$r \frac{dT}{dr} = c_1, \tag{B10}$$

$$\frac{dT}{dr} = \frac{c_1}{r}, \tag{B11}$$

$$T = c_1 \ln r + c_2, \tag{B12}$$

From Eq. (B12),

$$T_s - T_b = c_1(\ln r_s - \ln r_b) = c_1 \ln\left(\frac{r_s}{r_b}\right), \tag{B13}$$

and thus

$$c_1 = \frac{T_s - T_b}{\ln(r_s / r_b)}. \tag{B14}$$

The convective boundary condition equation for cylindrical geometry is,

$$-k_2 \left.\frac{dT}{dr}\right|_{r_s} = h(T_s - T_b). \tag{B15}$$

Substituting Eqs. (B11) and (B14) into (B15), we have

$$k_2 = h r_s \ln\left(\frac{r_b}{r_s}\right). \tag{B16}$$

B.3 Slab geometry

The heat conduction equation in slab geometry is, in a region free of heat source,

$$k_2 \frac{d^2T}{dx^2} = 0. \tag{B17}$$

Thus,

$$\frac{dT}{dx} = c_1, \tag{B18}$$

$$T = c_1 x + c_2, \tag{B19}$$

From Eq. (B19),

$$T_s - T_b = c_1(x_s - x_b), \tag{B20}$$

and thus

$$c_1 = \frac{T_s - T_b}{x_s - x_b}, \tag{B21}$$

The convection boundary condition equation for slab geometry is,

$$-k_2 \left.\frac{dT}{dr}\right|_{r_s} = h(T_s - T_b). \tag{B22}$$

Substituting Eqs. (B18) and (B21) into (B22), we have

$$k_2 = h(x_b - x_s). \tag{B23}$$

5. References

[1] H.S. Carslaw and J.C. Jaeger, *Conduction of Heat in Solids*, 2nd ed., Oxford (1959).

[2] T.M. Shih, *Numerical Heat Transfer*, Hemisphere Pub. Corp., Washington, D.C. (1984).

[3] S.V. Patankar, *Numerical Heat Transfer and Fluid Flow*, McGraw-Hill, New York (1980).

[4] P.E. MacDonald, et al, "NGNP Point Design–Results of the Initial Neutronics and Thermal-Hydraulic Assessments During FY-03", Idaho Natural Engineering and Environmental Laboratory, INEEL/EXT-03-00870 Rev. 1, September (2003).

[5] James J. Duderstadt and Louis J. Hamilton, *Nuclear Reactor Analysis*, John Wiley & Sons, Inc. (1976).

[6] Jun Shentu, Sunghwan Yun, and Nam Zin Cho, "A Monte Carlo Method for Solving Heat Conduction Problems with Complicated Geometry," *Nuclear Engineering and Technology*, 39, 207 (2007).

[7] Jae Hoon Song and Nam Zin Cho, "An Improved Monte Carlo Method Applied to the Heat Conduction Analysis of a Pebble with Dispersed Fuel Particles," *Nuclear Engineering and Technology*, 41, 279 (2009).

[8] Bum Hee Cho and Nam Zin Cho, "Monte Carlo Method Extended to Heat Transfer Problems with Non-Constant Temperature and Convection Boundary Conditions," *Nuclear Engineering and Technology*, 42, 65 (2010).

[9] X-5 Monte Carlo Team, "MCNP – A General Monte Carlo N-Particle Transfer Code, Version 5(Revised)", Los Alamos National Laboratory, LA_UR-03-1987 (2008).

[10] T.J. Hoffman and N.E. Bands, "Monte Carlo Surface Density Solution to the Dirichlet Heat Transfer Problem", *Nuclear Science and Engineering*, 59, 205-214 (1976).

[11] A. Haji-Sheikh and E.M. Sparrow, "The Solution of Heat Conduction Problems by Probability Methods", *ASME Journal of Heat Transfer*, 89, 121 (1967).

[12] T.J. Hoffman, "Monte Carlo Solution to Heat Conduction Problems with Internal Source", *Transactions of the American Nuclear Society*, 24, 181 (1976).

[13] S.K. Fraley, T.J. Hoffman, and P.N. Stevens, "A Monte Carlo Method of Solving Heat Conduction Problems", *Journal of Heat Transfer*, 102, 121(1980).

[14] Hui Yu and Nam Zin Cho, "Comparison of Monte Carlo Simulation Models for Randomly Distributed Particle Fuels in VHTR Fuel Elements", *Transactions of the American Nuclear Society*, 95, 719 (2006).

[15] Jae Hoon Song and Nam Zin Cho, "An Improved Monte Carlo Method Applied to Heat Conduction Problem of a Fuel Pebble", *Transaction of the Korean Nuclear Society Autumn Meeting*, Pyeongchang, (CD-ROM), Oct. 25-26, 2007.

[16] J. K. Carson, et al, "Thermal conductivity bounds for isotropic, porous material", *International Journal of Heat and Mass Transfer*, 48, 2150 (2005).

[17] C. H. Oh, et al, "Development Safety Analysis Codes and Experimental Validation for a Very High Temperature Gas-Cooled Reactor", INL/EXT-06-01362, Idaho National Laboratory (2006).

[18] Nam Zin Cho, Hui Yu, and Jong Woon Kim, "Two-Temperature Homogenized Model for Steady-State and Transient Thermal Analyses of a Pebble with Distributed Fuel Particles," *Annals of Nuclear Energy*, 36, 448 (2009); see also "Corrigendum to: Two-Temperature Homogenized Model for Steady-State and Transient Thermal

Analyses of a Pebble with Distributed Fuel Particles," *Annals of Nuclear Energy*, 37, 293 (2010).

[19] E.E. Lewis and W.F. Miller, Jr., *Computational Methods of Neutron Transport*, Chapter 7, John Wiley & Sons, New York (1984).

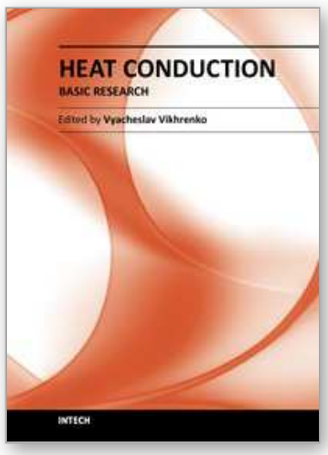

Heat Conduction - Basic Research

Edited by Prof. Vyacheslav Vikhrenko

ISBN 978-953-307-404-7
Hard cover, 350 pages
Publisher InTech
Published online 30, November, 2011
Published in print edition November, 2011

The content of this book covers several up-to-date approaches in the heat conduction theory such as inverse heat conduction problems, non-linear and non-classic heat conduction equations, coupled thermal and electromagnetic or mechanical effects and numerical methods for solving heat conduction equations as well. The book is comprised of 14 chapters divided into four sections. In the first section inverse heat conduction problems are discuss. The first two chapters of the second section are devoted to construction of analytical solutions of nonlinear heat conduction problems. In the last two chapters of this section wavelike solutions are attained.The third section is devoted to combined effects of heat conduction and electromagnetic interactions in plasmas or in pyroelectric material elastic deformations and hydrodynamics. Two chapters in the last section are dedicated to numerical methods for solving heat conduction problems.

InTech Europe
University Campus STeP Ri
Slavka Krautzeka 83/A
51000 Rijeka, Croatia
Phone: +385 (51) 770 447
Fax: +385 (51) 686 166
www.intechopen.com

InTech China
Unit 405, Office Block, Hotel Equatorial Shanghai
No.65, Yan An Road (West), Shanghai, 200040, China
中国上海市延安西路65号上海国际贵都大饭店办公楼405单元
Phone: +86-21-62489820
Fax: +86-21-62489821

IntechOpen